Electronic Supplementary Information (ESI):

Single-atom-sized Ni–N_4 site anchored in three-dimensional hierarchical carbon nanostructures for oxygen reduction reaction

Zhewei Cai,[a,b] Pan Du,[a,c] Wenhui Liang,[a] Hui Zhang,[a] Ping Wu,*[a] Chenxin Cai,*[a] and Zijie Yan*[b,d]

[a] Jiangsu Key Laboratory of New Power Batteries, Jiangsu Collaborative Innovation Center of Biomedical Functional Materials, College of Chemistry and Materials Science, Nanjing Normal University, Nanjing 210097, P.R. China.

[b] Department of Chemical and Biomolecular Engineering, Clarkson University, Potsdam, NY 13699, United States.

[c] College of Life Science and Chemistry, Jiangsu Second Normal University, Nanjing 210013, P. R. China.

[d] Department of Applied Physical Sciences, University of North Carolina at Chapel Hill, Chapel Hill, North Carolina 27599, United States.

*Corresponding Authors. E-mail: wuping@njnu.edu.cn (P.W.); cxcai@njnu.edu.cn (C.C.); zijieyan@unc.edu (Z.Y.)

Contents:

1. Calculation setups

The calculations were conducted using plane-wave spin-polarized density functional theory (DFT) as implemented in DmoL^3 code.[1,2] The Perdew-Burke-Ernzerhof (PBE)^3 exchange-correlation energy functional, which is a generalized gradient approximation (GGA) functional with Grimme methods for DFT-D correction, was used in the calculations. The convergence tolerance of energy, maximum force, maximum displacement, and Gaussian electron smearing width for the geometry optimization were set to 1.0×10^{-5} Hartree, 0.002 Hartree per Å, 0.005 Å, and 0.005 eV, respectively. We used a $4 \times 4 \times 1$ Monkhorst-Pack *k*-point mesh to sample the Brillouin zone.[4] A 5×5 monolayer graphene supercell, containing 60 carbon atoms, subjected to periodic boundary conditions, was constructed as a model system for calculation (Fig. S12).

For calculation of the formation energy (ΔE) of the Ni–N_4 or Ni–N_2, which are formed by binding Ni atom with four or two N atoms doped in carbon plane, the ΔE is defined in eqn. S1:

$$\Delta E = E_{\mathrm{Ni}} + E_{\mathrm{C–N4\ (or\ C–N2)}} - E_{\mathrm{Ni–N4\ (or\ Ni–N2)}} \qquad \text{(S1)}$$

where $E_{\mathrm{Ni–N4\ (or\ Ni–N2)}}$ is the energy of the optimized Ni–N_4 or Ni–N_2; $E_{\mathrm{C–N4\ (or\ C–N4)}}$ is the energy of the optimized four N atoms (or two N atoms) doped carbon; and E_{Ni} is the energy of the isolated Ni atom in gas phase. In this definition, a positive value of ΔE represents energetically favorable process, implying the product is stable.

The ΔE of the Ni–EMIM (binding of the Ni^{2+} ion with EMIM cations) and Ni–dca (binding of the Ni^{2+} ion with dca anions) was calculated based on this definition in eqn. S1.

For calculation of the adsorption of O_2 and the related intermediates involved in the ORR, the adsorption energy (E_{ad}) is defined in eqn. S2:

$$E_{\mathrm{ad}} = E_{\mathrm{t}} - E_0 - E_{\mathrm{x}} \qquad \text{(S2)}$$

where E_{t}, E_0, and E_{x} are the total energy of the total adsorbed system including the adsorbed species (O_2, and the related intermediates) and NiN_4–C, the energy of the NiN_4–C catalyst, and the energy of the isolated adsorbed species, respectively. In this definition, a negative value of E_{ad} represents an exothermic adsorption process, suggesting the adsorption is energetically favorable.

The free-energy diagram of the ORR was calculated based on a computational hydrogen electrode (CHE) model,[5] which declares that the chemical potential of a proton/electron ($H^+ + e^-$) in solution is equal to half the chemical potential of a gaseous H_2. The reference electrode was set up to be the NHE. The change in free energy (ΔG) of each reaction step is calculated based on eqn. S3:

$$\Delta G = \Delta E + \Delta \mathrm{ZPE} - T\Delta S + \Delta G_{\mathrm{U}} + \Delta G_{\mathrm{pH}} \qquad \text{(S3)}$$

where ΔE is the reaction energy associated with the reactant and product molecules adsorbed on the catalytic surface in each ORR step, ΔZPE is the change in zero-point energies (ZPE), T is the temperature which refers to room temperature ($T = 298.15$ K), and ΔS is the change in entropy. The ZPEs and entropies of the ORR intermediates are calculated from vibrational frequencies and those of gas phase molecules are obtained from the standard thermodynamic database. The effect of an external bias (ΔG_{U}) is to shift ΔG by $-eU$ in each ($H^+ + e^-$) transfer step, where e is the number of electrons transferred and U is the applied bias. $\Delta G_{\mathrm{pH}} = k_{\mathrm{B}}T\ln 10 \times \mathrm{pH}$ where k_{B} is Boltzmann's constant and the pH value is set to 13 because the electrochemical measurements were performed in 0.1 M KOH solution.

2. Synthesis and characterization of the NiN_4–C catalysts

In a typical synthesis, 570 mg EMIM-dca (>98.5%, Sigma-Aldrich) was mixed with 100 mg $Ni(NO_3)_2$ (the concentration of $Ni(NO_3)_2$ in the mixture was 15 wt.%) by vigorously stirring overnight until a homogeneous mixture was achieved. The mixture was then transferred to a corundum crucible, which was placed in center of a tube furnace, for pyrolysis under an atmosphere of inert gas (high-purity Ar gas). The mixture was first heated by ramping the temperature to 900 °C at 5 °C/min and then keeping it at 900 °C for 2 h to complete the pyrolysis. The furnace was turned to off and the temperature was allowed to cool down naturally to ambient temperature.

The as-synthesized catalysts were purified by overnight refluxing in 100 mL H_2SO_4 solution (2 M) in air at 110 °C to remove any metallic Ni and nickel oxide particles produced during pyrolysis, heating in forming gas (Ar/10% H_2) at a temperature of 900 °C for 2 h, and refluxing in 2 M H_2SO_4 solution in a similar way as the first refluxing step. After each refluxing step, the suspensions were filtered and washed with distilled water until the filtrate exhibited a pH value of ~7. The catalyst was finally obtained after drying the filter cakes in air at 80 °C.

The aim of these purifying procedures is to thoroughly remove the metallic Ni and nickel oxide particles, which are wrapped in the carbon layers. These particles can block the reactant (O_2 molecules) from the active sites, making it difficult to identify the active sites and causing the catalytic mechanism of the ORR to change. The procedure only removes the free-standing Ni and nickel oxide particles but not changes the Ni–N_4 sites that are stably embedded and bonded in carbon layers. A 10% H_2 (volume ratio) was introduced into the atmosphere of Ar gas in the second heating procedure to reduce any oxidized nitrogen species and the oxidized Ni atom in the structure of Ni–N_4. These oxidized species may be formed in the refluxing steps in H_2SO_4 solution in air at 110 °C.

The heating and refluxing procedures cause serious loss of catalyst mass, thus, the mass yield of the final catalyst is low (40–50% in this work), which is a common feature of catalysts prepared by pyrolysis.

To study the effects of the nickel salt content and the pyrolysis temperature on the catalytic activities and active sites of the NiN_4–C catalysts, the catalysts were synthesized by changing the nickel salt content

from 5 to 15 wt% in the synthesis mixture while keeping the pyrolysis temperature at 900 °C, and the pyrolysis temperature was varied between 700 and 1000 °C while keeping the nickel salt content at 15 wt%.

The N–C catalyst (without Ni) was synthesized by pyrolyzing the EMIM-dca at 900 °C and treated with acid using the same steps as those for the synthesis of NiN_4–C catalysts. The Ni–C catalyst (without nitrogen) and carbon catalyst (both Ni and N free) were synthesized by pyrolysis of a mixture of $Ni(NO_3)_2$ and glucose (with 15 wt% of $Co(NO_3)_2$ in the mixture), and glucose, respectively, using the same steps as those for the synthesis of NiN_4–C catalyst.

XPS was measured with an ESCALAB 250 XPS spectrometer (VG Scientifics) using a monochromatic Al Kα line at 1486.6 eV. Binding energies were calibrated with respect to the C1s peak at 284.6 eV. Raman spectra were measured on a Labram HR 800 microspectrometer (Jobin Yvon) with an excitation source of 514 nm. XRD patterns were recorded on a Rigaku/Max-3A X-ray diffractometer with Cu Kα radiation (λ = 0.15418 nm). The morphologies of the synthesized NiN_4–C catalysts were observed on a JEOL JEM-2100F TEM. The sub-Ångström-resolution, aberration-corrected HAADF–STEM images were recorded on a JEOL JEM 2200FS STEM/TEM, equipped with a CEOS (Heidelburg, Ger) probe corrector, with a nominal image resolution of 0.07 nm. The amount of Ni in the catalysts was quantitatively determined via ICP-OES using an Optima 7300 DV (PerkinElmer). The specific surface areas (BET surface areas) of the catalysts were calculated based on the nitrogen sorption isotherms, which were measured using a Quadrasorb MP porosimetry apparatus (Quantachrome). The X-ray absorption spectra (XAS) were measured at BL14W1 station in Shanghai Synchrotron Radiation Facility (SSRF). The electron storage ring of SSRF was operated at 3.5 GeV, with a maximum current of 250 mA. EXAFS data were collected on fluorescence mode, and the energy was calibrated using Ni foil. Utilizing the ATHENA module of the IFEFFIT software packages, the obtained EXAFS data were performed according to the standard procedures.

3. Electrochemical measurements

The electrochemical measurements were performed with an RRDE technique in a three-electrode cell at an ambient temperature. An RRDE (Pine Research Instrumentation) was used as the working electrode. The RRDE electrode consisted of a catalyst-coated glassy carbon (GC) disk (with a diameter of 5.61 mm and an electrode area of 0.2472 cm^2) surround by a Pt ring (0.1856 cm^2 in area, with inner and outer ring diameters of 6.25 and 7.92 mm, respectively). A platinum wire and an Ag/AgCl electrode (saturated with KCl solution) were used as the counter electrode and reference electrode, respectively. The data were recorded using a Pine Wave Driver (bipotentiostat, Pine Research Instrumentation). The supporting electrolyte was 0.1 M KOH aqueous solution (AR grade) prepared with ultrapure water (18.2 MΩ cm). All electrode potentials in this work are referenced to NHE by adding a value of 0.197 V to the potentials measured versus the Ag/AgCl reference electrode.

To immobilize the catalyst on the electrode surface, 12 mg of the synthesized catalyst powder was ultrasonically dispersed in a mixed solvent containing 450 μL of water, 500 μL of ethanol, and 50 μL of 5 wt.% Nafion solution, and then ten microliters of the ink was cast onto the GC disk surface, and the solvent was allowed to evaporate in air at an ambient temperature, resulting in a catalyst loading of 0.12 mg (~0.49 mg/cm^2) on the electrode surface, which corresponds to ~20 $\mu g_{Ni}/cm^2$ (the content of Ni atoms in the catalyst is ~4 wt.% as estimated by ICP-OES).

The ORR activity was measured in the O_2-saturated 0.1 M KOH solution. The CVs were recorded on the disk electrode at 50 mV/s. CV collected in an argon-saturated electrolyte serves as a blank. The linear sweep voltammetry (LSV) polarization curves were recorded via cathodic scans of the GC disk electrode potential from 0.3 to –0.5 V at 5 mV/s with varying rotating speed from 400 to 3600 rpm. Current densities (mA/cm^2) were normalized using the ECSA. The i_k and, subsequently, the k for the ORR were derived from Koutecky-Levich plots (eqns. S4–S6).

$$\frac{1}{i} = \frac{1}{i_K} + \frac{1}{i_L} = \frac{1}{i_K} + \frac{1}{B\omega^{1/2}} \quad \text{(S4)}$$

$$B = 0.62nFC_0D_0^{2/3}\nu^{-1/6} \quad \text{(S5)}$$

$$i_K = nFkC_0 \quad \text{(S6)}$$

where i is the measured current density, i_K and i_L are the kinetic- and diffusion-limiting current densities, ω is the angular velocity of the disk ($\omega = 2\pi f$, where f is the linear rotation speed), n is the number of electrons transferred per O_2 molecule, F is the Faraday constant (96485 C/mol), C_0 is the bulk concentration of O_2 (1.18×10^{-6} mol/mL), v is the kinematic viscosity of the electrolyte (0.01 cm^2/s), D_0 is the O_2 diffusion coefficient (1.93×10^{-5} cm^2/s), and k is the electron-transfer rate constant. The value of n and i_k can be obtained from the slope and intercept of the Koutecky-Levich plots, respectively.

A Tafel analysis was performed between the i_K and η (in V) for the ORR polarization on the NiN_4–C catalyst surface using eqn. S7

$$\eta = a + b \log i_K \quad \text{(S7)}$$

where a (in V) is the Tafel constant and b (in V/dec) is the Tafel slope.

The selectivity for water formation at the NiN_4–C catalyst was measured using two different techniques: (i) the Koutecky-Levich technique where half-cell measurements are performed at different rotating speeds to obtain n, the total number of electrons passing during the ORR reaction, and (ii) RRDE experiments where the Pt ring was held at a potential of 0.5 V (vs. NHE), which is high enough to oxidize any OOH^- intermediates produced on the GC disk electrode during the ORR process. The value of n (a value of $n = 4$ corresponds to a complete $4e^-$ reduction of O_2 to water, whereas a value of $n = 2$ is a $2e^-$ reduction of O_2 to H_2O_2) and the OOH^- intermediate production percentage (OOH^-%, which serves as the $2e^-$ pathway selectivity) were determined via eqn. S8 and eqn. S9, respectively.

$$n = 4 \times \frac{i_D}{i_D + \frac{i_R}{N}} \quad \text{(S8)}$$

$$OOH^- \% = 200 \times \frac{\frac{i_R}{N}}{i_D + \frac{i_R}{N}} \quad \text{(S9)}$$

where i_D is the disk current, i_R is the ring current, and N is the collection efficiency of the RRDE (which is 37% in this work as specified by the manufacturer).

The accelerated durability tests (ADTs) were performed at room temperature in N_2-saturated 0.1 M KOH solution by applying cyclic potential sweeps between –0.2 and 0.2 V versus NHE at a sweep rate of 200 mV/s for 10000 cycles. The LSV polarization curves in the O_2-saturated 0.1 M KOH solution were recorded before and after ADTs at 1600 rpm and a scanning rate of 5 mV/s.

4. TOF calculation

The TOF value of the NiN_4–C catalyst was calculated from the basic relation between TOF, the catalyst mass-normalized ORR activity (i_K), and the catalyst mass-normalized active site density (SD), given as

i_K (in A g^{-1}) = e (in C $electron^{-1}$) × TOF (in electron $site^{-1}$ s^{-1}) × SD (in site g^{-1})

where the i_K is the kinetic current at 0.1 V (vs NHE. This potential is about 0.88 V if the RHE is used a reference electrode), e is elementary electron charge (1.6×10^{-19} C $electron^{-1}$), TOF is the turnover frequency in units of electrons transferred per site and per second, and SD the mass-normalized density of accessible active sites on the surface.

The mass-based SD is estimated from the mass content of Ni in the catalyst, which was determined using ICP-OES, and assuming that every Ni atom in the catalyst has formed the Ni–N_4 structures (active site). It should be noted that the estimated SD value in this way is much higher than that actually involved in the catalytic reaction because the estimated value represents the total active site in catalyst, however, only those active sites on the catalyst surface can participate in the reaction.

5. Fabrication of single cell zinc-air battery

A home-made Zinc-air battery device has been employed for the battery performance. The electrolyte used for zinc-air battery was 6 M KOH and 0.2 M $Zn(Ac)_2$ solution. Typically, 4 mg NiN_4–C catalysts mixed with 40 μL Nafion solution (5 wt%) were dispersed in 1 mL of water-isopropanol solution with volume ratio of 3:1 by sonicating for at least 1 h to form a homogeneous ink, a certain volume of catalyst ink was then brushed onto a 1 cm^2 carbon paper (HCP020) with a catalyst loading of 1.25 mg/cm. A polished zinc plate was used as the anode. As a reference material, 20 wt% Pt/C catalysts were prepared as the same procedure.

6. Tables

Table S1. Fitting parameters of NiN_4–C catalyst EXAFS spectra including coordination number (N), interatomic distance (R), Debye-Waller factor (σ^2), and energy shift (E_0).

path	N	R (Å)	σ^2 (Å^2)	E_0 (eV)
Ni–N	4	1.87	0.002	4.73

Table S2. Comparison of the ORR kinetic parameters for the NiN_4–C and commercial Pt/C catalysts in 0.1 M KOH solution [a]

catalyst	U_{onset} (V vs. NHE)	$U_{1/2}$ (V vs. NHE)	i_K [b] (mA/cm^2)	k (cm/s)
NiN_4–C	0.20	0.11	6.55	1.42×10^{-2}
Pt/C	0.20	0.10	6.40	1.40×10^{-2}

[a] The loading of the NiN_4–C and commercial Pt/C catalysts on the electrode surface was 0.49 mg/cm^2 and 20 μg_{Pt}/cm^2, respectively.

[b] The values of i_K (at 0.1 V vs. NHE) were calculated based on the Koutecky-Levich plot (eqn. S4).

Table S3. Comparison of ORR activities of NiN_4–C catalyst with other recently reported non-noble-metal catalyst in alkaline medium.

Catalyst [a]	**Loading** [b] **(mg / cm^2)**	**Electrolyte**	$U_{1/2}$ [c] **(V vs RHE)**	**Reference**
NiN_4–C	0.49	0.1 M KOH	0.86	This work
CrN	0.20	0.1 M KOH	0.53	*ACS Catal.*, 2016, **6**, 6165.
Cu_3N/C	0.49	0.1 M KOH	0.68	*ACS Appl. Nano Mater.*, 2018, **1**, 3673.
$V_{0.95}Co_{0.05}N$	0.61	0.1 M KOH	0.76	*ChemSusChem*, 2017, **10**, 68.
Ti-Ni-N/C	0.50	0.1 M KOH	0.80	*J. Mater. Chem. A*, 2015, **3**, 16801.
Co-N_x-C graphene	0.25	0.1 M KOH	0.80	*Adv. Mater.*, 2017, 1703185.
p-Fe-N-CNFs	0.60	0.1 M KOH	0.82	*Energy Environ. Sci.*, 2018, **11**, 2208.
Fe_3C@Fe-N-doped CNFs	0.60	0.1 M KOH	0.82	*Angew. Chem.*, 2017, **127**, 8297.
Fe-N-DSC	0.10	0.1 M KOH	0.83	*ACS Nano*, 2018, **12**, 208.
Fe/NMC-11	0.51	0.1 M KOH	0.84	*Adv. Energy Mater.*, 2017, 1701154.
Co-doped ZIFs	0.80	0.1 M KOH	0.85	*Adv. Mater.*, 2018, 1706758.
C-FeHZ8@g-C_3N_4-950	0.51	0.1 M KOH	0.85	*J. Mater. Chem. A*, 2019, **7**, 5020.
S,N-Fe/N/C-CNT	0.60	0.1 M KOH	0.85	*Angew. Chem. Int. Ed.*, 2017, **56**, 610.
Fe-ISAS/CN	0.51	0.1 M KOH	0.86	*Chem. Sci.*, 2020, **11**, 786.
Co_3N/C	0.26	1 M KOH	0.86	*J. Am. Chem. Soc.*, 2019, **141**, 19241.
Co_2N/C	0.26	1 M KOH	0.86	*J. Am. Chem. Soc.*, 2019, **141**, 19241.
Fe-N-C HNSs	0.26	0.1 M KOH	0.87	*Adv. Mater.*, 2018, 1806312.
Fe-N-SCCFs	1.0	0.1 M KOH	0.88	*Nano Lett.*, 2017, **17**, 2003.
Fe-N_4 SAs/NPC	0.50	0.1 M KOH	0.89	*Angew. Chem. Int. Ed.*, 2018, **57**, 8614.
Fe-ISAs/CN	0.31	1 M KOH	0.90	*Nano Energy*, 2017, **32**, 353.
Fe SAs/N-C	0.25	0.1 M KOH	0.91	*ACS Catal.*, 2019, **9**, 2158.

[a] refer to the each reference for the full name of the catalyst.

[b] estimated based on the procedures of the electrode fabrication reported in each reference.

[c] half-wave potential, reported against RHE (reversible hydrogen electrode) here.

7. Figures

Fig. S1 The color changes of the EMIM-dca IL after addition of $Ni(NO_3)_2$. (a) Pure EMIM-dca; (b) Mixture of EMIM-dca and $Ni(NO_3)_2$ taken after $Ni(NO_3)_2$ dissolved immediately without stirring; and (c) Mixture of EMIM-dca and $Ni(NO_3)_2$ after stirred overnight.

When the nickel salt was added into EMIM-dca and strongly stirred overnight, the color of the EMIM-dca changed from faint yellow to green and cyan blue, implying the Ni^{2+} ions have bound with EMIM-dca.

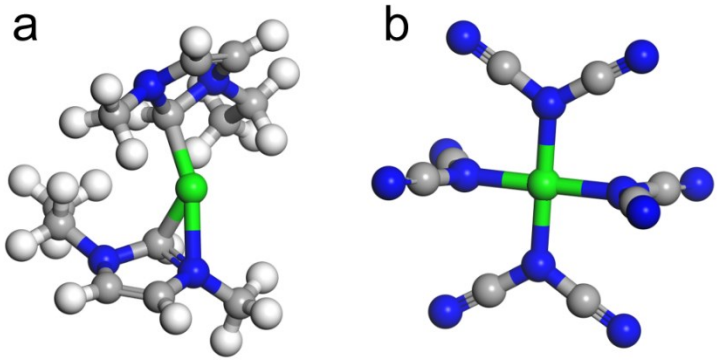

Fig. S2 Side view of the optimized configuration of the Ni^{2+} ion binding with EMIM cation (a) and dca anion (b). Atomic color code: gray, carbon; blue, nitrogen; green, nickel; and white, hydrogen atom.

Our theoretical simulation shows that the Ni^{2+} ions can be bound with both imidazolium (EMIM) cation (via formation of two Ni–C bonds and one Ni–N bonds) and dca anion (forming Ni–dca, via formation of the four Ni–N bonds). However, the formation energy of the Ni–EMIM is ~3.1 eV lower than that of the Ni–dca, implying that the binding of Ni^{2+} with dca anion is dominant in the mixture. This result has been further confirmed by the IR spectrum of the mixture (Fig. S3).

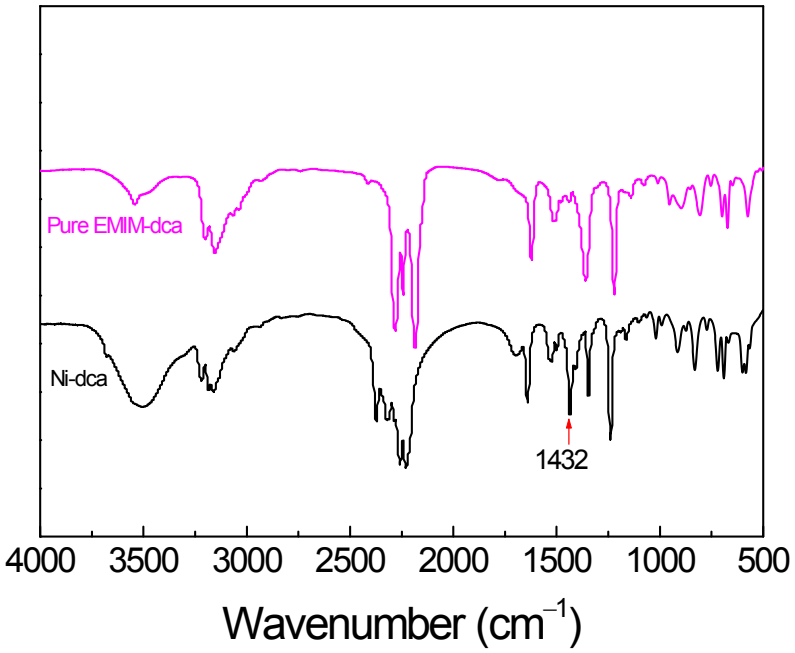

Fig. S3 IR spectra of pure EMIM-dca and Ni–dca complex.

In comparison with the pure EMIM-dca, there is a new strong absorption peak at ~1430 cm^{-1}, which is the characteristic absorption of Ni–N bond. Observation of this peak in the IR spectrum of the mixture suggests the formation of the Ni–N bond between the Ni^{2+} and dca. However, no characteristic absorption of the Ni–C bond (should be at ~1940 cm^{-1}) can be observed in its IR spectrum, indicating there is no Ni–C bond formation. These results further demonstrate that the Ni^{2+} ions preferentially bind to dca anion via forming the Ni–N bonds, rather than to EMIM cations, agreeing well with the theoretical simulations (Fig. S2).

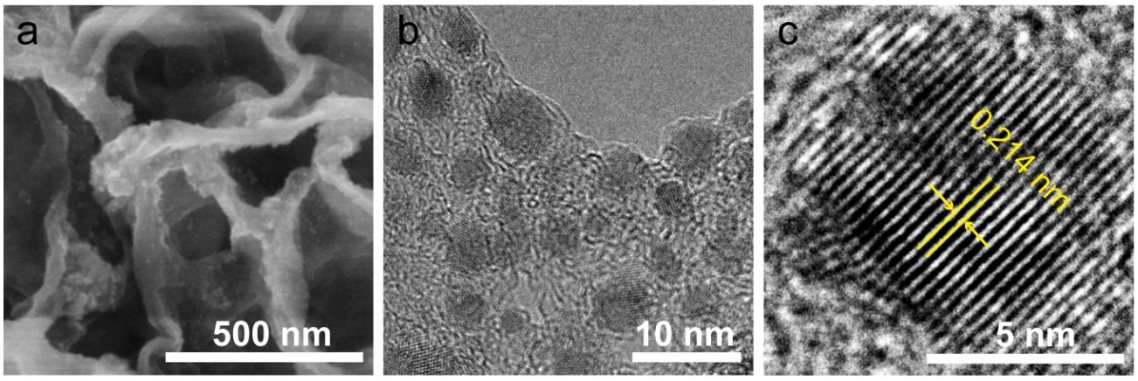

Fig. S4 SEM (a) and TEM (b, c) images of the as-synthesized NiN_4–C catalyst before purification (acid leaching). There are many small particles with sizes of about ~5 nm in diameter wrapped in the carbon layers as shown in image (a) and (b). HRTEM image (c) indicate that these small particles have a high crystallinity with a lattice spacing of ~0.214 nm (image c), which is ascribed to the (110) plane of metallic Ni.

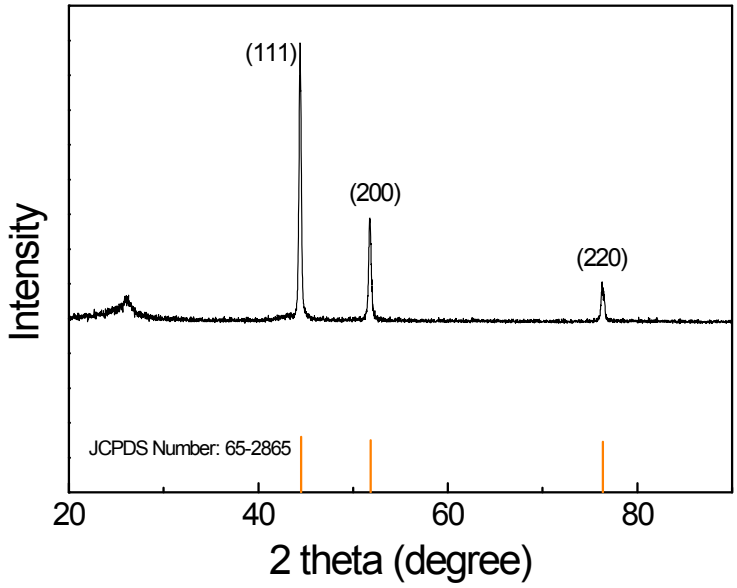

Fig. S5 XRD patterns of the unpurified NiN_4–C catalysts, which show strong diffraction peaks of (111), (200), and (220) planes of metallic Ni at ~44.5, 51.9, and 76.5 degrees (JCPDS number 65-2865).

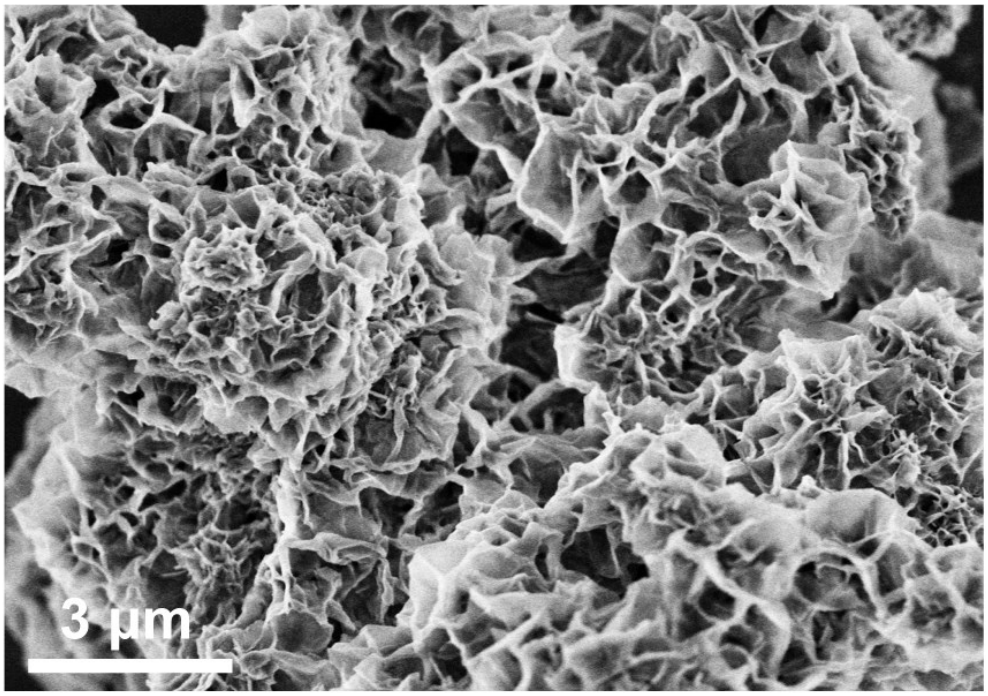

Fig. S6 SEM image of the purified NiN_4–C catalysts at low magnification, suggesting that such a hierarchical structure can be synthesized with a high yields.

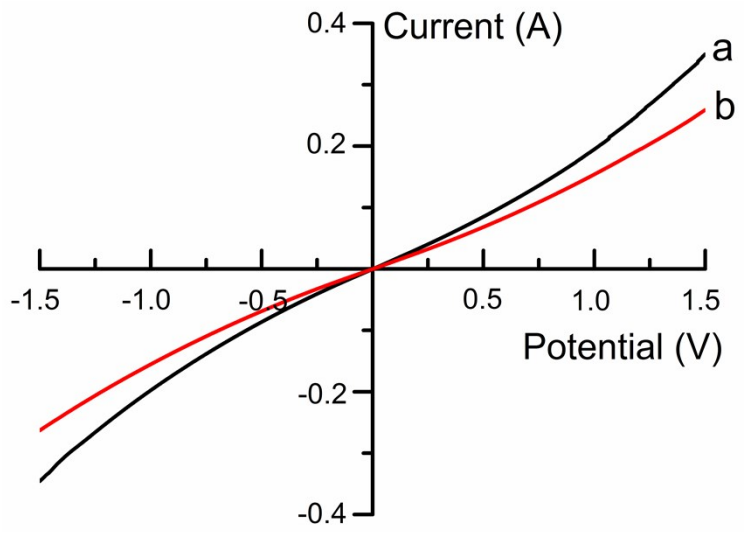

Fig. S7 *I–V* curves for NiN_4–C (a) and N–C (b). Scan rate: 100 mV/s.

The electrical conductivity of the NiN_4–C catalyst and N–C was estimated from DC measurements. The samples (NiN_4–C and N–C) were pressed to the rods by a homemade two-electrode cell template (0.4 cm in diameter and 8.5 cm in length) under 20 MPa. Then, the rods of NiN_4–C and N–C were performed the current-voltage (*I–V*) measurements on a CHI 760B electrochemical workstation. The voltage was scanned from –1.5 to 1.5 V with no applied gate voltage at 100 mV/s. The current response was recorded. The values of the electrical conductivity (σ) were calculated according the following equation:

$$\sigma = \frac{I}{V}\frac{l}{A}$$

where A is the surface area of the samples rod (in m^2), l is the length of samples (in m), and the value I/V was taken as the slope of *I–V* curves. The calculated σ of NiN_4–C and N–C is ~2.52 × 10^3 S $m^{-1}$and 1.01 × 10^3 S m^{-1}, respectively.

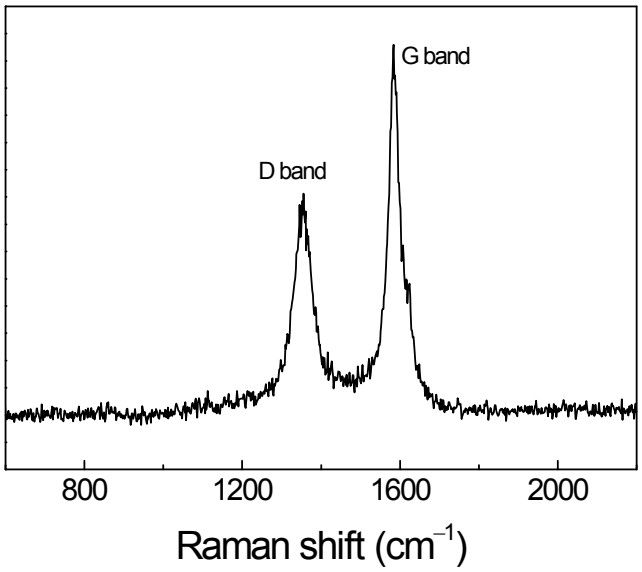

Fig. S8 Raman spectrum of the NiN_4–C catalysts, showing the sharp and well-separated G and D peaks at ~1592 and 1347 cm^{-1}, respectively, with a high intensity ratio (I_G/I_D) of ~1.6.

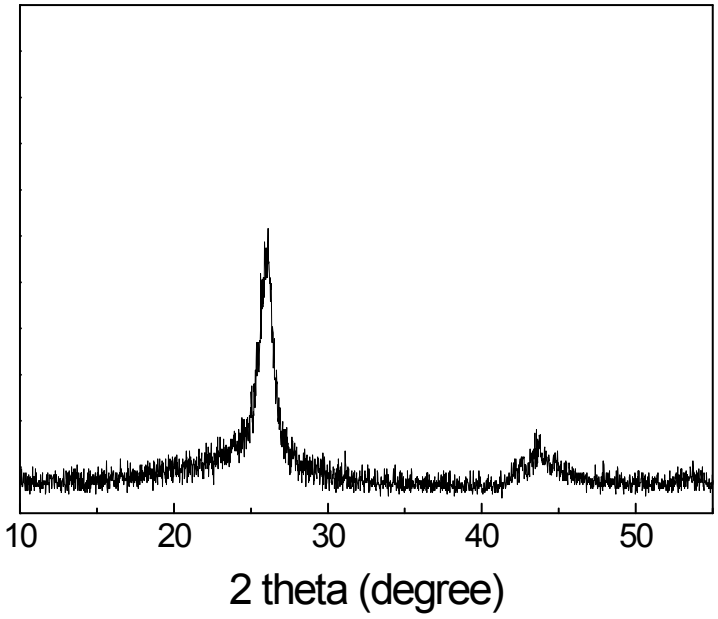

Fig. S9 XRD patterns of the purified NiN_4–C catalysts, showing the well-defined patterns of graphite carbon plane of (002) and (101) at ~26.2 and 43.6 degrees, respectively. No XRD patterns related to Ni particles are observed.

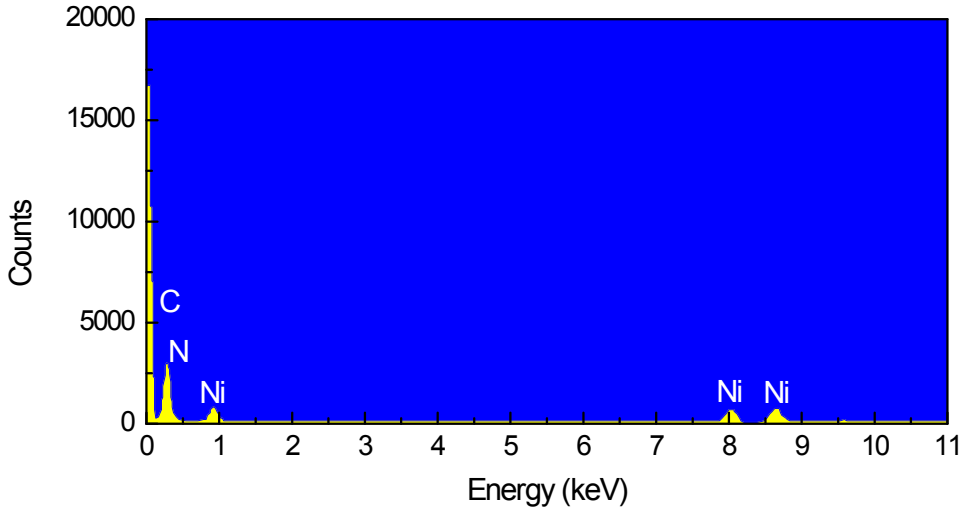

Fig. S10 EDS of the purified NiN_4–C catalysts.

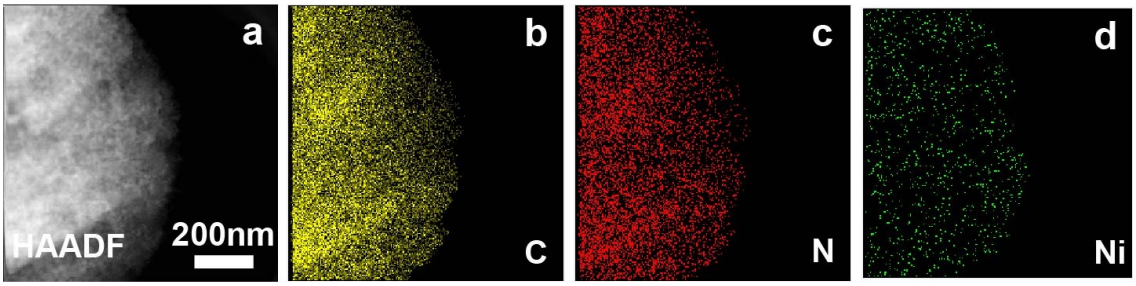

Fig. S11 HAADF–STEM image of the NiN_4–C catalysts (a), and the corresponding elemental mapping for C (b), N (c), and Ni (d). The mapping of the element distribution of the catalyst indicates the existence of Ni element; moreover, the Ni element uniformly distributes on the catalyst surface. The Ni element is mapped using the spectral line of ~8.6 keV (see Fig. S9).

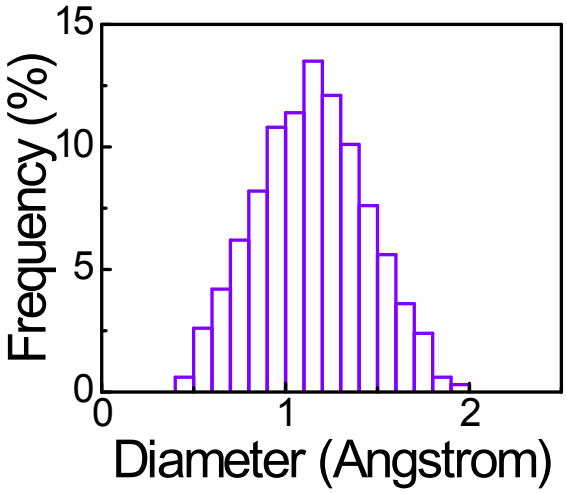

Fig. S12 The size distribution of the Ni atoms on the catalysts. The size distribution were analyzed based on measured sizes of at least 100 bight dots. The size of each bright dots was measured using Nano Measure software, a software developed for particle size measurement.

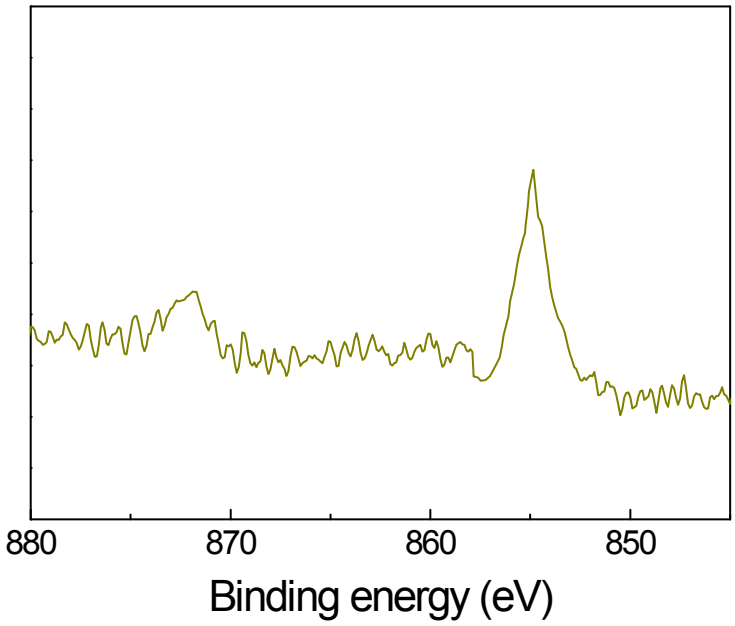

Fig. S13 High-resolution XPS spectrum of the Ni 2p in the NiN_4–C catalysts, showing a Ni $2p_{3/2}$ peak at ~854.2 eV.

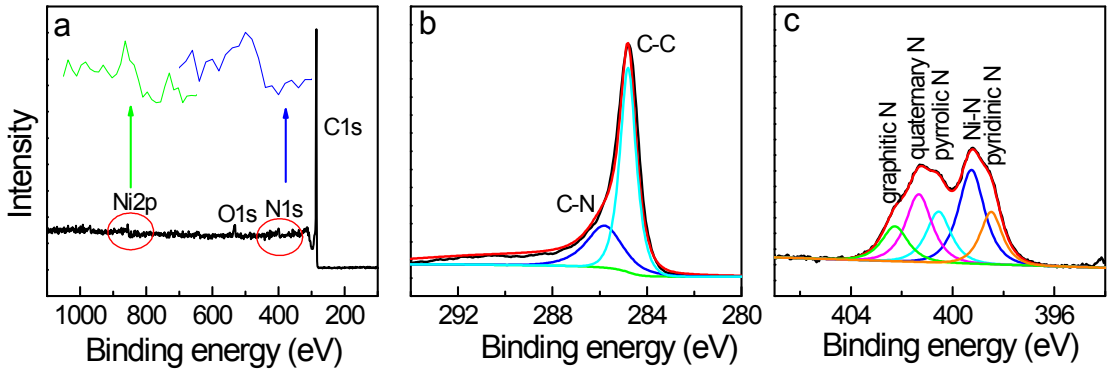

Fig. S14 (a) XPS spectrum of the synthesized Ni–N_4 catalyst. The inset shows the amplified XPS of Ni2p and N1s. (b, c) High-resolution XPS spectra of the C1s (b), and N1s (c), respectively, and their related curve-fitted components.

The survey XPS spectrum shows the presence of carbon, nitrogen, oxygen, and Ni elements. The presence of the oxygen is a typical phenomenon as the surface of carbon materials tends to be oxidized slightly when handled under ambient conditions. The C1s core level spectrum has an asymmetrical shape. The two dominant contributions to the spectrum at ~284.8 and 285.8 eV are of higher significance. At ~284.8 eV, carbon atoms that neighbor other carbon atoms in a sp^2 binding environment are represented, while at the higher binding energy (~285.8 eV), carbon atoms are bound to more electronegative binding partners (here, this can be ascribed to the presence of nitrogen-bound carbon atoms).

The core level spectrum of N1s shows that the N1s core level spectrum has an asymmetrical shape and thus a broadened contribution. It can be confirmed the presence of pyridinic (~398.5 eV), pyrrolic (~400.6 eV), quaternary (~401.3 eV), and graphitic N (~402.3 eV). When we decompose the N1s peak, another peak with a high intensity that is shifted up by ~0.8 eV from the binding energy of pyridinic N has to be included in the fit. This corresponds to the binding energy at ~399.3 eV. This is the energy of the nitrogen bond to metal, the Ni–N bond here, which is in good agreement with the results obtained from XANES and theoretical simulation.

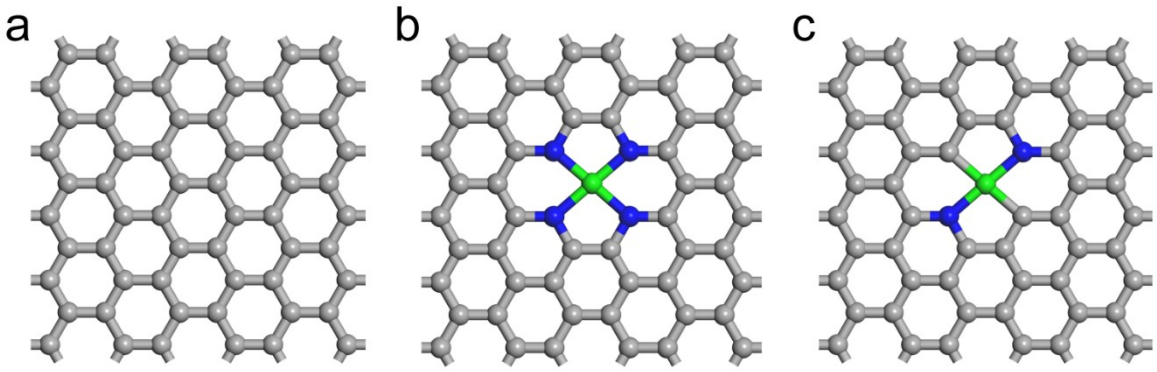

Fig. S15 (a) The 5 × 5 monolayer graphene model cell, which contains 60 carbon atoms, used for calculations; (b, c) top view of the optimized configurations of the Ni–N_4 (b) and Ni–N_2 (c) structures. Atomic color code: gray, carbon; blue, nitrogen; green, nickel; and white, hydrogen atom.

The optimized pristine graphene sheet has an in-plane C–C bond length of 1.42 Å, which agrees well with previous computations and the in-plane C–C distance in graphite. After the N atom was doped into the graphene sheet, the Ni atom can theoretically coordinate with N atoms in the forms of Ni–N_4 or Ni–N_2. Our calculation showed the formation energy (ΔE) of Ni–N_4 is ~2.94 eV higher than that of Ni–N_2 (ΔE for Ni–N_4 and Ni–N_2 is about 4.27 and 1.33 eV, respectively), implying Ni in the catalyst prefers to bind with four N atoms, i.e., Ni–N_4 is the dominant form, agreeing well with the experimental results derived from the simulations of the EXAFS spectra.

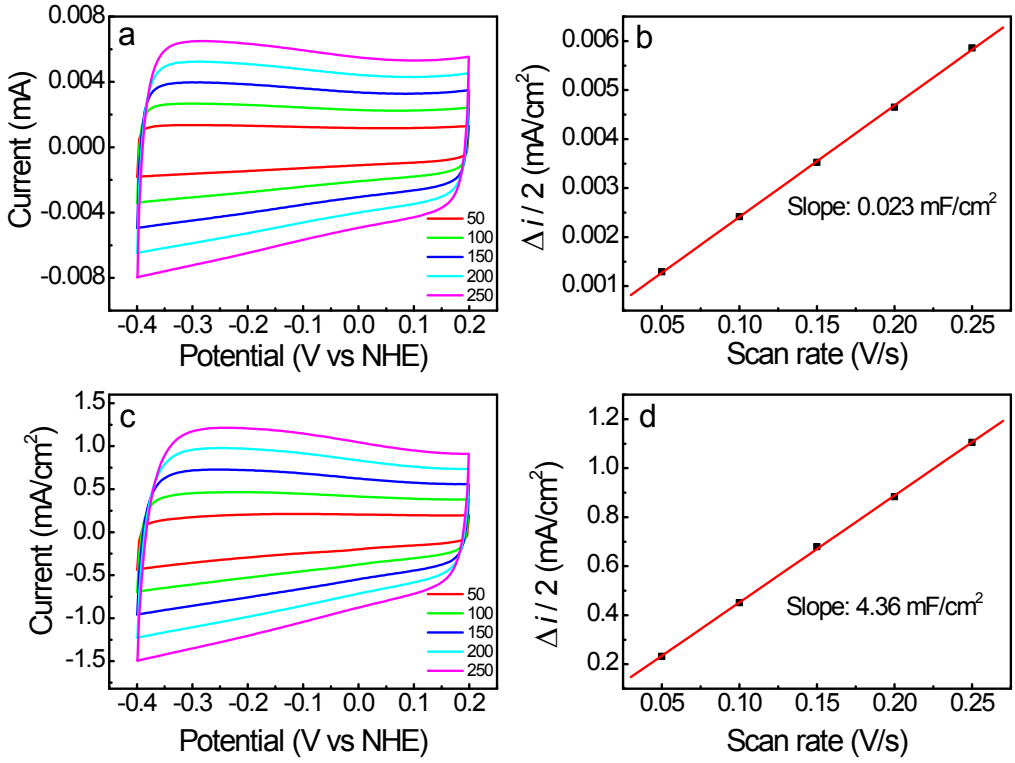

Fig. S16 CV of bare GC electrode (a) and the GC coated with NiN_4–C catalyst (c) with the catalyst loading of ~0.50 mg/cm^2 at different scanning rates. (b, d) The dependence of the double-layer charge current against scanning rates for bare GC electrode (b) and the GC coated with NiN_4–C catalyst (d).

The ECSA was estimated from the dependence of the double-layer charge current against scanning rates. The measured electrochemical double layer capacitance (EDLC) of bare GC electrode was ~23 μF/cm^2, close to the reported graphene value of ~ 21 μF/cm^2.[6] The EDLC of the catalyst on the GC electrode was estimated to be ~4.36 mF/cm^2, which corresponds to ECSA of 39.1 m^2/g.

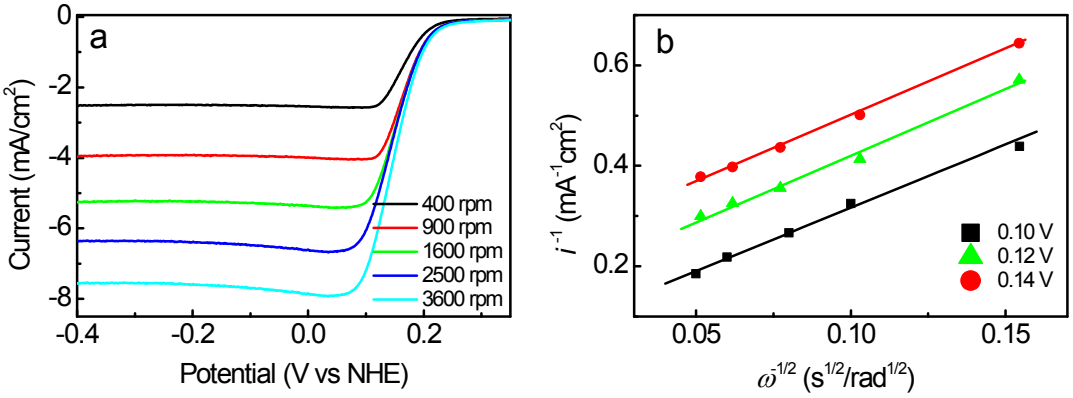

Fig. S17 ORR polarization curves obtained in O_2-saturated 0.1 M KOH solution for the NiN_4–C catalysts at different rotating speeds (a) and their related Koutecky-Levich plot at different potentials (b).

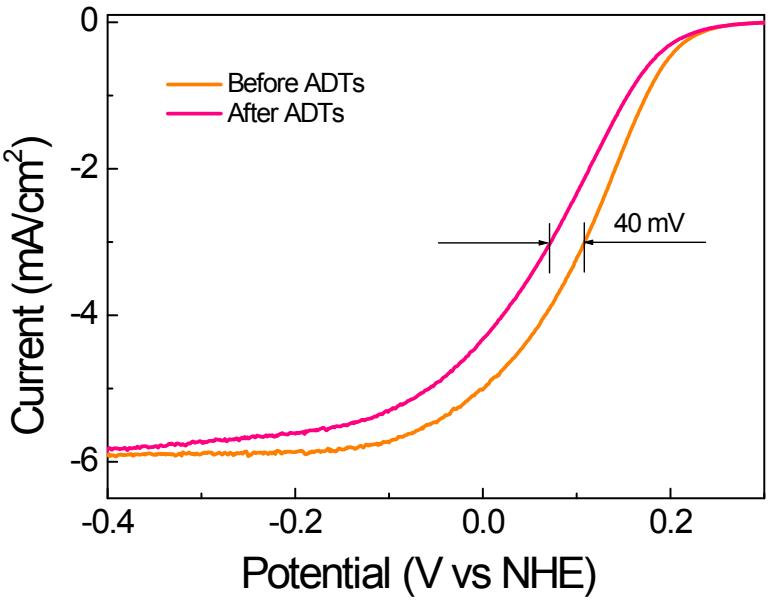

Fig. S18 The stability of the commercial Pt/C catalyst to ORR. The RDE responses were recorded in O_2-saturated 0.1 M KOH solution at a rotating speed of 1600 rpm and a scanning rate of 5 mV/s before and after ADTs. The ADTs measurements were performed by potential cycling of the catalyst between –0.2 and 0.2 V versus NHE at 200 mV/s in a N_2-saturated 0.1 M KOH solution for 10000 cycles. The results showed that there is the negative shifts of 40 and 20 mV for the $U_{1/2}$ and U_{onset}, respectively, after the ADTs; moreover, i_K also decreases by ~15%.

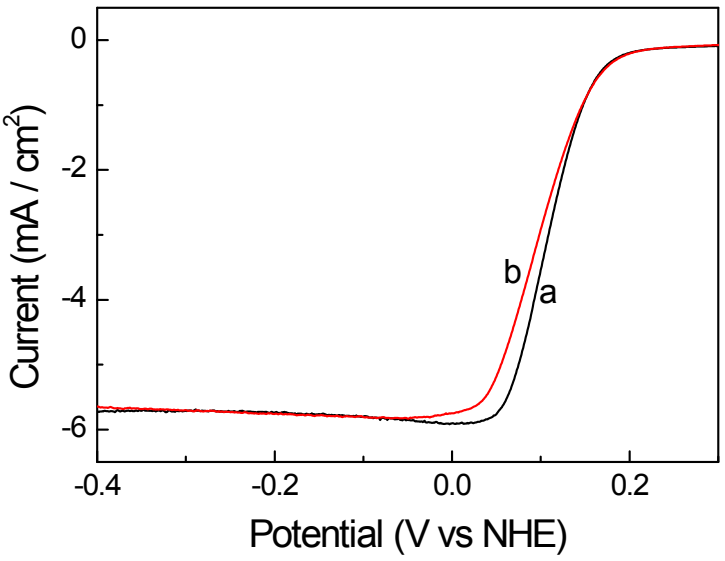

Fig. S19 The stability of resistance of the NiN_4–C catalyst to the crossover effect of CH_3OH. The RDE responses were recorded in O_2-saturated 0.1 M KOH solution at a rotating speed of 1600 rpm and a scanning rate of 5 mV/s in the absence (a) and presence of 3 M CH_3OH. The results indicate that no obvious change in the activity (for example, U_{onset} and the diffusion limited current are almost same) can be identified in the presence and absence of 3 M CH_3OH except the $U_{1/2}$ has a ~10 mV negative shift in the CH_3OH-containing solution, implying high tolerance ability of the catalyst to the CH_3OH crossover effect.

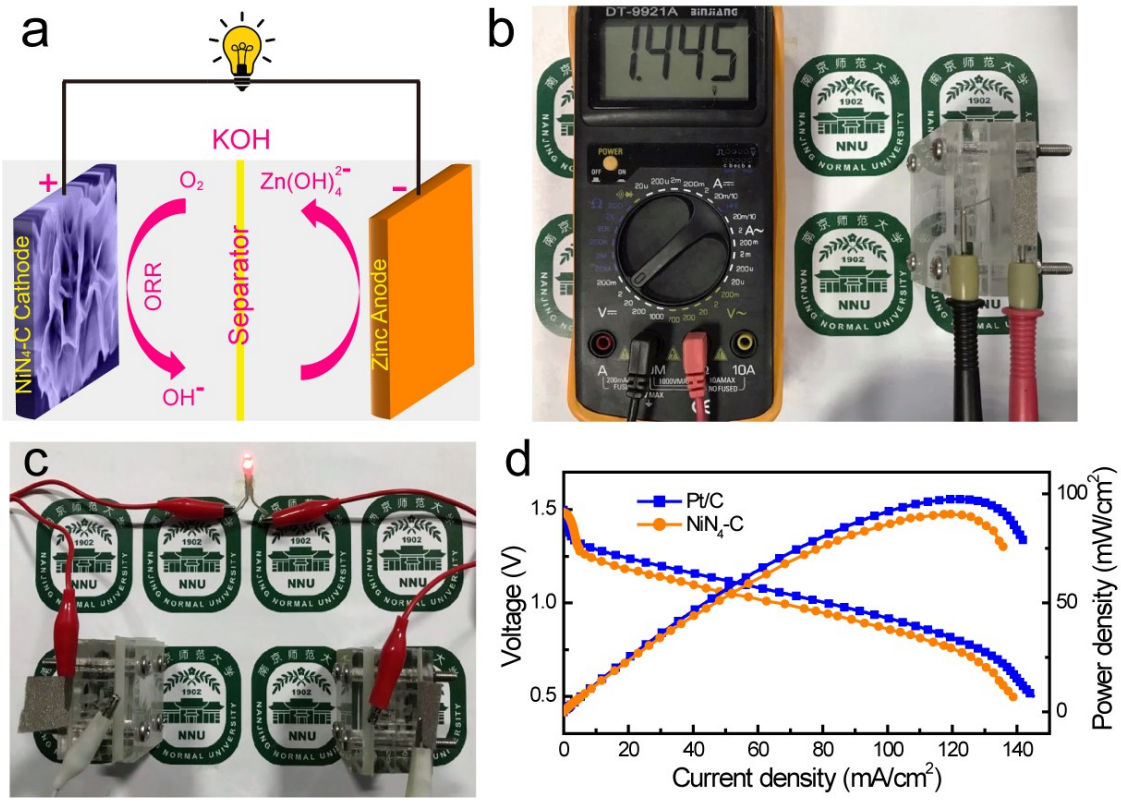

Fig. S20 Electrochemical performance of NiN_4–C catalyst in a homemade Zn-air battery. (a) Schematic configuration of the Zn-air battery. (b) Photo image showing the open circuit voltage of ~1.45 V for the NiN_4–C catalyst-based Zn-air battery. (c) Photo image showing two the NiN_4–C catalyst-based Zn-air batteries can light up a bulb with a working voltage of 3 V. (d) Discharge polarization curves and corresponding power density plots for NiN_4–C and Pt/C catalyst-based Zn-air batteries.

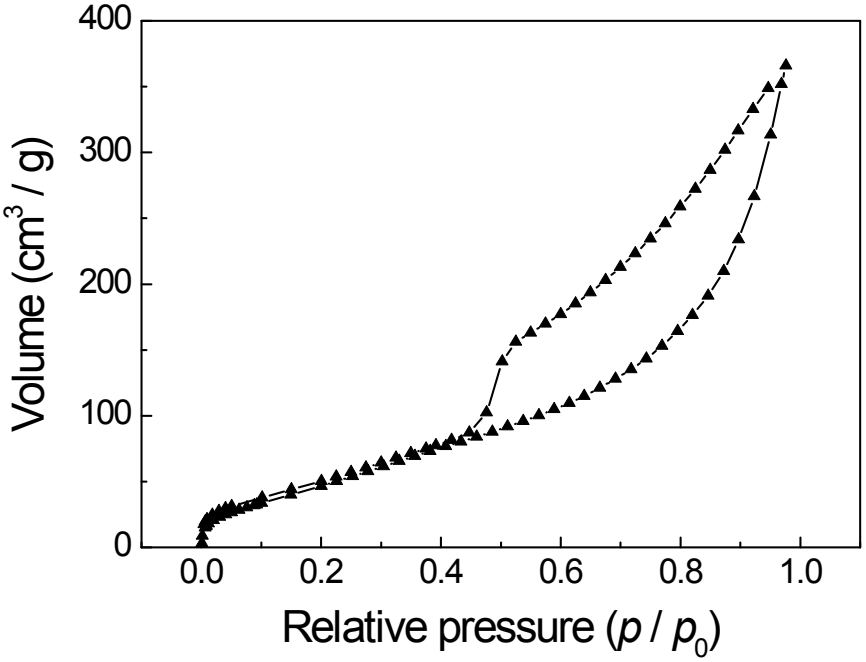

Fig. S21 Nitrogen sorption isotherms of NiN_4–C catalysts.

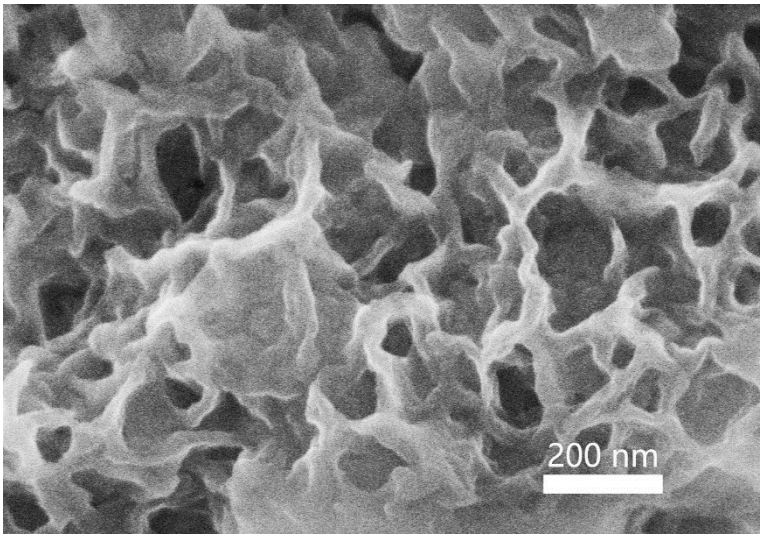

Fig. S22 SEM image of the N–C catalysts. It shows that the N–C catalysts have the similar 3D hierarchical structure to NiN_4–C catalyst.

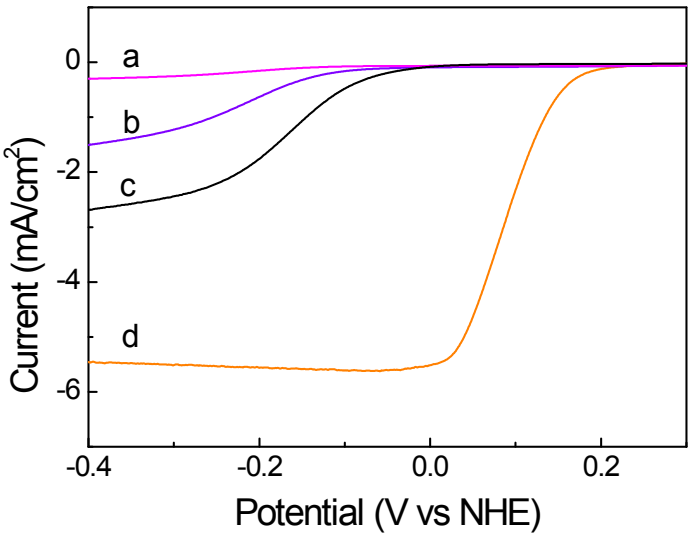

Fig. S23 RDE measurements in O_2-saturated 0.1 M KOH solution for the carbon (a), N–C (b), Ni–C (c), and NiN_4–C catalysts (d). The measurements were performed at ambient temperature with a rotating speed of 1600 rpm and a scanning rate of 5 mV/s. The loading of the catalyst was ~0.49 mg/cm^2.

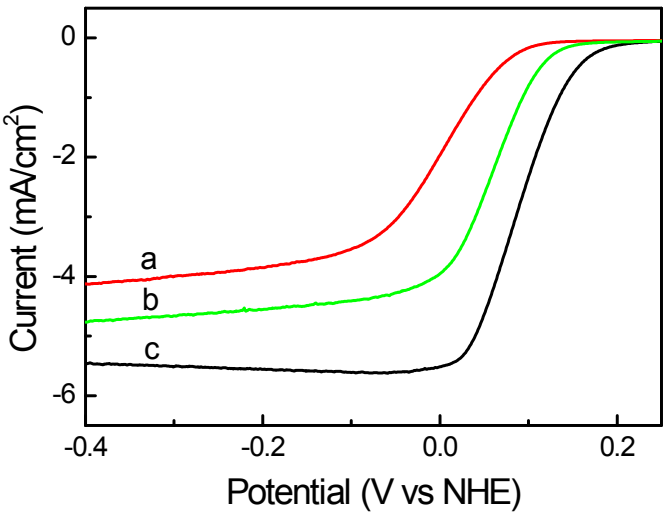

Fig. S24 RDE measurements in O_2-saturated 0.1 M KOH solution for the NiN_4–C catalyst synthesized under the pyrolysis temperature of 900 °C with initial Ni salt content of (a) 5, (b) 10, and (c) 15 wt% in the synthesis mixture. The measurements were performed at ambient temperature with a rotating speed of 1600 rpm and a scanning rate of 5 mV/s. The loading of the catalyst was 0.49 mg/cm^2.

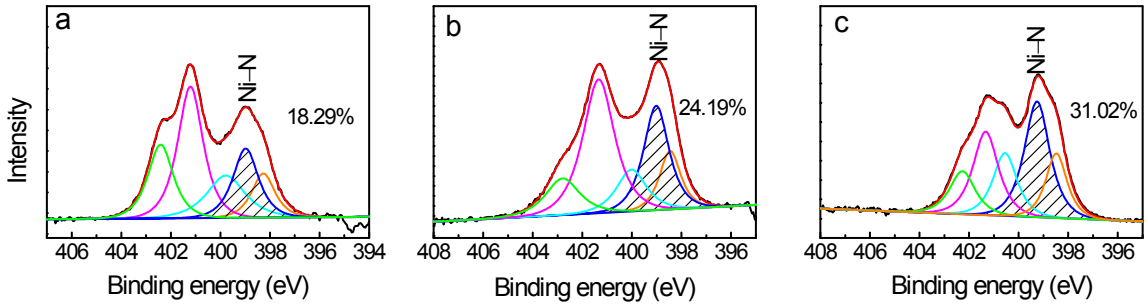

Fig. S25 High-resolution XPS spectra of N1s and their related curve-fitted components in the NiN_4–C catalyst synthesized under the pyrolysis temperature of 900 °C with initial Ni salt content of (a) 5, (b) 10, and (c) 15 wt% in the synthesis mixture. The number marked in each panel indicates the percentage of Ni–N species in the total amount of N species content.

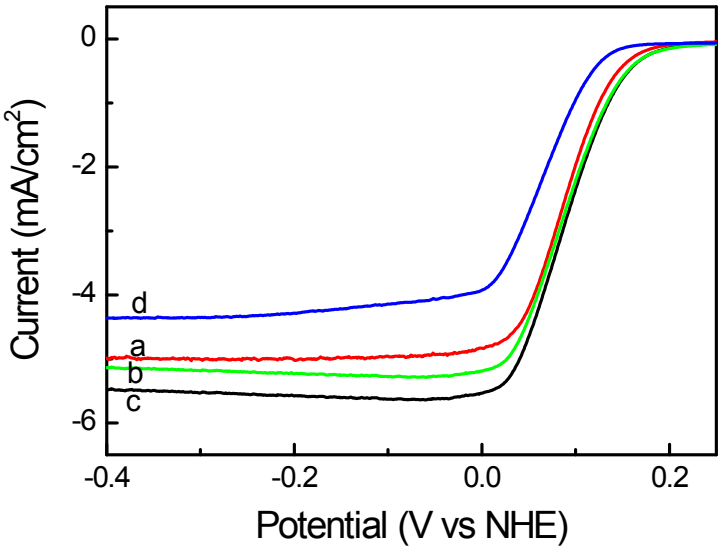

Fig. S26 RDE measurements in O_2-saturated 0.1 M KOH solution for the NiN_4–C catalyst synthesized under the pyrolysis temperature of (a) 700, (b) 800, (c) 900, and (d) 1000 °C with initial Ni salt content of 15 wt% in the synthesis mixture. The measurements were performed at ambient temperature with a rotating speed of 1600 rpm and a scanning rate of 5 mV/s. The loading of the catalyst was 0.49 mg/cm^2.

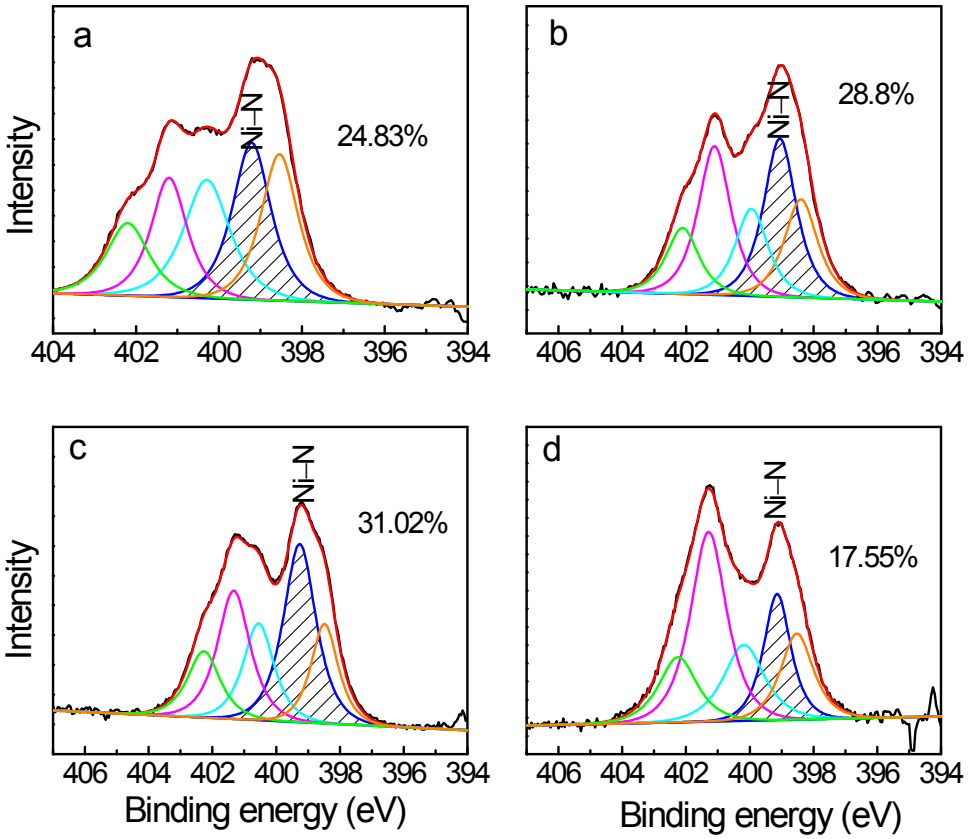

Fig. S27 High-resolution XPS spectra of N1s and their related curve-fitted components in the NiN_4–C catalyst synthesized under the pyrolysis temperature of (a) 700, (b) 800, (c) 900, and (d) 1000 °C with the Ni salt content in the synthesis mixture keeping at constant of 15 wt%. The number marked in each panel indicates the percentage of Ni–N species in the total amount of N species content.

8. References

1 B. Delley, *J. Chem. Phys.*, 2000, **113**, 7756–7764.

2 J. P. Perdew, K. Burke and M. Ernzerhof, *Phys. Rev. Lett.*, 1996, **77**, 3865–3868.

3 H. J. Monkhorst and J. D. Pack, *Phys. Rev. B: Solid State*, 1976, **13**, 5188–5192.

4 J. Nørskov, J. Rossmeisl, A. Logadottir, L. Lindqvist, J. Kitchin, T. Bligaard and H. Jonsson, *J. Phys. Chem. B*, 2004, **108**, 17886–17892.

5 M. Newville, *J. Synchrotron Rad.*, 2001, **8**, 322–324.

6 J. Chen, C. Li and G. Shi, *J. Phys. Chem. Lett.*, 2013, **4**, 1244–1253.